ROYAL SOCIETY OF CHEMISTRY

PAPER

Anisotropic growth of gold nanoparticles using cationic gemini surfactants: effects of structure variations in head and tail groups†

Titoo Jain,[a] Ali R. Tehrani-Bagha,[b] Himanshu Shekhar,[c] Ross Crawford,[c] Erik Johnson,[a] Kasper Nørgaard,[a] Krister Holmberg,[b] Paul Erhart[c] and Kasper Moth-Poulsen*[b]

A library of gemini surfactants is employed to study surfactant directed anisotropic growth of gold nanoparticles. The surfactants are modified with respect to the length and type of the tails, as well as of the spacer group. By analyzing the structure of the anisotropic nanoparticles, it is possible to extract information on how the structure of the surfactants influences the anisotropic gold nanocrystal growth. We find that the tail length of the surfactants has a greater influence on the resulting nanoparticle aspect ratio compared to the chemical nature of the spacer group. While clear trends between the aspect ratio and the tail as well as spacer length remain elusive, we observe that surfactants with a critical micelle concentration of ~1 mM produce particles with the highest aspect ratio. A crystallographic analysis of nanorods obtained using gemini surfactants reveals that they grow along $\langle 100 \rangle$ and are bound by $\{310\}$ facets. This observation, which is specific for gemini surfactants, is explained by taking into account the preferential alignment of gemini surfactants with surface steps as suggested by electronic structure calculations.

Introduction

Anisotropic noble metal nanostructures are of general interest due to their attractive optical and physical properties.[1,2] Gold nanorods have been employed in several applications including plasmonic sensors,[3,4] advanced therapeutics,[5,6] self-assembly[7,8] and molecular electronics.[9–13] One of the most widely used synthetic methods for the preparation of anisotropic gold nanorods (AuNRs) is the surfactant assisted, seed-mediated growth procedure.[14,15] The most common surfactant employed in this context is cetyltrimethylammonium bromide ($C_{16}TAB$), for which the effects of temperature,[16] pH,[17,18] counter-ions[19,20] and small amounts of silver ions[21,15] on the resulting AuNRs have been explored. Examples of variations in surfactant type and structure are much more scarce, and typically only a small number of surfactants are tested in each study.[22–24] The effect of the head and tail group chemical structures on the formation of anisotropic metal nanostructures thus remains an open question.

The actual growth process is highly complex involving a wealth of different thermodynamic and kinetic components; hence it is not surprising that a thorough understanding has so far been elusive. A comprehensive description of Au nanorod growth would have to account for example for entropic effects (especially related to the configurational disorder associated with the long hydrocarbon tails), solvation effects (related to the chemical potential of the constituents), and kinetic effects, as well as for the details of the adsorption process (geometry, charge transfer, and energetics). So far only a few studies have been conducted in this area including molecular dynamics simulation studies based on empirical potentials[25,26] as well as thermodynamic approaches.[27] While such approaches are valuable for obtaining a general picture they treat the interaction between surface and surfactant in an approximate way.

Several mechanisms have been proposed to explain the physical origin of the surfactant guided growth of anisotropic nanostructures including: (1) the "zipping mechanism", in which the dynamic formation of a surfactant bilayer on Au surfaces promotes anisotropic AuNR growth by providing a template structure.[24] (2) "Differential surfactant binding" to different crystallographic faces, where the cationic surfactant preferentially binds to the $\{100\}$ and $\{110\}$ side-facets of the Au crystal leading to the growth of the $\{111\}$ end-facet.[28] (3) "Underpotential deposition" where silver ions preferentially adsorb on the high-energy side-facets allowing for faster Au reduction on unblocked end-facets.[21] Synthetic methods and growth mechanisms have been frequently discussed in the literature and we refer to a recent review.[2]

[a]Nano Science Center, Department of Chemistry, University of Copenhagen, Denmark
[b]Department of Chemical and Biological Engineering, Chalmers University of Technology, Gothenburg, Sweden
[c]Department of Applied Physics, Chalmers University of Technology, Gothenburg, Sweden. E-mail: Kasper.Moth-Poulsen@Chalmers.se
† Electronic supplementary information (ESI) available: Additional TEM images of the anisotropic gold particles. DOI: 10.1039/c3tc32057j

The length of the surfactant tail is known to be critical for anisotropic gold nanoparticle growth.[24] The van der Waals interactions between the long tails render bilayer formation energetically more favorable and thereby stabilize bilayers. This observation in fact motivated the proposition of the zipping mechanism referred to above.

The present work is motivated by the question whether the surfactant structure can be optimized to further enhance the bilayer stability and in turn lead to even larger aspect ratios. Specifically, we consider cationic gemini surfactants with short spacer units, which are known to form long elongated micelles above their critical micelle concentration (CMC),[29,30] this renders them prime candidates for the formation of AuNRs through solution-based approaches.[22,31,32] The goal is to establish structure–property relationships that might guide future design of surfactants for anisotropic nanocrystal growth. We examine a series of 12 gemini surfactants having both simple alkane and ester-containing tails of different lengths. The spacer length is also varied and in two of the surfactants a hydroxyl group is introduced in the spacer unit in order to increase its polarity. The conventional monomeric surfactant CTAB is used as a reference.

The resulting Au nanoparticles are characterized using absorption spectroscopy and transmission electron microscopy (TEM) in which both selected area and confined beam electron diffraction (SAED) are performed. Based on the TEM data, a detailed size-determination analysis is performed, and the results are discussed in the context of the structure of the gemini surfactants.

We find that among the 4 studied surfactants that lead to anisotropic crystal growth (AR > 2), all but one has a critical micelle concentration close to 1 mM (Fig. 3).

Further we observe that gold nanorods obtained using gemini surfactants grow along ⟨100⟩ and are confined by {310} surfaces. This contrasts with the {110} and {250} facets observed in the case of CTAB mediated growth.[31] The emergence of {310} side facets is explained on the basis of electronic structure calculations, which provide evidence that gemini surfactants stabilize and align surface steps with {310} surfaces being {100} surfaces with large step densities.

Experimental section

Materials

For gold particle synthesis: cetyltrimethylammonium bromide (CTAB, 99%), sodium tetrahydridoborate (NaBH$_4$, 99%), silver nitrate (AgNO$_3$, 99.8%), and hydrogen tetrachloroaurate(III) trihydrate (HAuCl$_4$, 99.9%) were obtained from Aldrich Chemicals. Ascorbic acid was obtained from Merck. All reagents were used as received and all glassware was thoroughly cleaned with a solution of sulfuric acid and potassium chlorate before use.

For filtration of surfactant solutions a PVDF SLGVX13NL syringe filter (0.22 µM, 13 mm, non-sterile) was obtained from Fisher.

All solutions are aqueous and water was purified using a Millipore-MilliQ setup for ultrapure water (18.2 MΩ cm).

Synthesis of surfactants

The synthesis routes for preparation of alkyl-based and ester-containing cationic gemini surfactants have been reported in the literature.[33–37] The cationic geminis with short spacers (2 methylene groups) were prepared by reaction of a long chain alkyl bromide with *N,N,N′,N′*-tetramethyl-1,2-ethanediamine. The other cationic geminis were synthesized by reaction of a long chain tertiary amine with the corresponding dibromoalkane.

Critical micelle concentration (CMC)

The conductivity of varying concentrations of the cationic surfactants in water was measured with a CDM 210 conductometer (Radiometer, France) in a temperature-controlled double-walled glass container with water circulation. For each series of measurements an exact volume of 10 mL Millipore water (resistivity 18.2 MΩ cm) was introduced into the vessel and the specific conductivity of the water was recorded. The conductivity was measured at constant temperature (21 °C) while the solutions were titrated successively by adding surfactant solution of known concentration. The conductance was measured after thorough mixing and temperature equilibration after each addition.[34]

It is known that the specific conductivity changes linearly with the surfactant concentration, with a break at the CMC. The intersection point between the two straight lines gives the CMC and the difference in the slopes is due to binding of some of the counterions to the micelle. The micelle ionization degree (α) is obtained as the ratio of the slopes above and below the CMC.[38]

Synthesis of gold nanoparticles

The AuNR synthesis follows the seed-mediated growth approach with reaction conditions similar to what is used for CTAB-capped gold nanorods.[39] In a typical experiment, gold nanoparticle seeds with a size of 2–3 nm were prepared by adding 0.6 mL 0.01 M of ice cold NaBH$_4$ solution to an aqueous mixture of 7.5 mL 0.1 M CTAB and 0.25 mL 0.01 M HAuCl$_4$. Addition of NaBH$_4$ immediately induced a color change from the orange CTA$^+$–AuCl$_4^-$ complex to brown suggesting the formation of nanoparticles. The mixture was stirred and shaken vigorously for 2 min and left to mature for at least 2 hours at 27 °C before further use. In our study, we chose to keep the seeds constant using the procedure well-known to produce optimal AuNR solutions for the CTAB-assisted method.[40] Employing gemini surfactants in the seed synthesis may alter the outcome and may be the subject of future investigations.

A growth solution of 4.75 mL gemini surfactant, 0.2 mL of 0.01 M HAuCl$_4$, 30 µL of 0.01 M AgNO$_3$, and 32 µL of 0.1 M ascorbic acid was prepared. A loss of color is observed when adding ascorbic acid due to Au reduction (Au^{3+} to Au^{1+}). Finally, 21 µL of the matured gold nanoparticle seeds were added to the growth solution and the solution was left undisturbed for 24 h at 27 °C. During the first hour of growth the color of the solutions changed to various shades of blue, purple and red depending on the surfactant and, thus, the resulting particle shapes and dimensions.

The gemini surfactants were prepared in concentrations corresponding to 50 times their respective CMC values. The aqueous surfactant solutions were sonicated at 35 °C for at least 30 minutes and filtered through a 0.22 μM syringe filter before being stabilized at 27 °C and used for nanoparticle growth.

Some gemini surfactants were initially tested at much lower concentrations (e.g. 10 and 20 times CMC) without finding any qualitative change in the results, concluding that small concentration changes due to the filtration would not lead to a noticeable change in the observed results.

Purification of the nanoparticles was accomplished by two rounds of centrifugation (20 min at 5600 × g). After each round the supernatant was exchanged with 1 mL of 100 μM of the respective surfactant.

Absorption spectroscopy

Absorption spectra were obtained on a Perkin Elmer Lambda 1050. A Hellma Analytics Quartz SUPRASIL cuvette with a path length of 1 cm was used. For a typical measurement, the nanoparticle solution was diluted 7-fold in 100 μM of the respective surfactant.

Electron microscopy and particle analysis

For transmission electron microscopy imaging, a droplet (3 μL) of sample solution was cast on a formvar carbon-coated copper grid and left to evaporate. Images and SAED/CBID patterns were acquired on a Philips CM20 instrument operated at 200 kV with an Olympus Veleta 2k × 2k side-mounted CCD camera.

Particle analysis for size determination was performed on TEM images acquired with a resolution of at least 0.6 nm per pixel using the ImageJ software package. For each sample, 1000–8000 particles were analyzed by fitting to an ellipse. In the case of square particles or rods of a rectangular shape (in the 2D projection), a correction factor of $\sqrt{\pi}/2$ was used to rectify overestimation caused by the elliptical fitting in ImageJ.[41] Particles with an aspect ratio above 1.25 are defined as being rod-shaped particles and the rod-yield, η_{AuNR}, is given by $\eta_{AuNR} = N_{AR>1.25}/(N_{AR>1.25} + N_{AR\leq1.25})$.

Computational model

Calculations were carried out within density functional theory using the projector augmented wave method[42,43] as implemented in the Vienna ab initio simulation package.[44–46] We employed a plane wave energy cutoff of 320 eV and sampled the Brillouin zone using k-point grids with a density comparable to a Γ-centered 15 × 15 × 15 k-point grid with respect to the primitive face-centered cubic cell of Au. The generalized gradient approximation parametrized by Perdew, Burke, and Ernzerhof[47] was employed to represent the exchange–correlation potential. A detailed account of the calculation method and results will be published elsewhere.
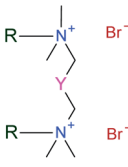
Results

General observations

The effects of structural variations in a library of gemini surfactants on the anisotropic growth of gold nanoparticles are examined. Eight gemini surfactants with straight alkane chain tails and four with ester containing tails have been studied and are shown in Table 1 with their respective CMC values. The variables in the chemical structure of the surfactants are: (a) the alkyl chain length, (b) the spacer length, (c) the presence of an ester bond in the alkyl tails, and (d) the presence of a hydroxyl group in the spacer. The CMC value of a gemini surfactant is at least one order of magnitude lower than the value of the corresponding single chain surfactant.[33,48,49] The CMC values of the geminis were found to be dependent mostly on the alkyl chain length, while other variables in the chemical structure have a relatively small effect. The presence of an ester bond in the alkyl chains increases the CMC 2–3 times (compare 9E2Q-3-Q2E9 with 12Q-3-Q12 and 9E2Q-3(OH)-Q2E9 with 12Q-3(OH)-Q12).

A higher CMC is an indication of self-assembly in bulk solution being energetically less favorable. Self-assembly into micelles, admicelles or double layers on surfaces is a phenomenon similar to self-assembly in bulk. Thus, it is expected that ester-containing geminis self-assemble somewhat less readily than the non-ester containing geminis with the same number of carbon atoms on a gold crystal surface.

Table 1 Chemical structure and CMC values of the cationic gemini surfactants used in this study. Q and E represent quaternary head group and ester bond, respectively

Chemical structure	Alkyl tail	Spacer	Abbreviation	CMC [mM] (21 °C)
	$R = CH_3-(CH_2)_9-$	$Y = -$	10Q-2-Q10	6.3
	$R = CH_3-(CH_2)_{11}-$	$Y = -$	12Q-2-Q12	0.85
	$R = CH_3-(CH_2)_{11}-$	$Y = CH_2$	12Q-3-Q12	0.89
	$R = CH_3-(CH_2)_{11}-$	$Y = CH_2-OH$	12Q-3(OH)-Q12	0.72
$R-\overset{\mid}{\underset{\mid}{N^+}}$ Br⁻	$R = CH_3-(CH_2)_{11}-$	$Y = (CH_2)_2$	12Q-4-Q12	1.10
Y	$R = CH_3-(CH_2)_{11}-$	$Y = (CH_2)_4$	12Q-6-Q12	1.15
$R-\overset{\mid}{\underset{\mid}{N^+}}$ Br⁻	$R = CH_3-(CH_2)_{13}-$	$Y = -$	14Q-2-Q14	0.15
	$R = CH_3-(CH_2)_{13}-$	$Y = (CH_2)_2$	14Q-4-Q14	0.21
	$R = CH_3-(CH_2)_8-COO-(CH_2)_2-$	$Y = CH_2$	9E2Q-3-Q2E9	2.1
	$R = CH_3-(CH_2)_8-COO-(CH_2)_2-$	$Y = CH_2-OH$	9E2Q-3(OH)-Q2E9	1.8
	$R = CH_3-(CH_2)_8-COO-(CH_2)_2-$	$Y = (CH_2)_4$	9E2Q-6-Q2E9	2.6
	$R = CH_3-(CH_2)_{10}-COO-(CH_2)_2-$	$Y = CH_2$	11E2Q-3-Q2E11	0.31

In general the influence of the spacer length and the nature on the CMC is small. For example going from a 3-carbon spacer to a 6-carbon spacer in otherwise identical structures (9E2Q-3-Q2E9 and 9E2Q-6-Q2E9) slightly increases the CMC. Similar results are obtained for non-ester containing surfactants (14Q-2-Q14 and 14Q-4-14Q). Note that the diminishing effect of the spacer length on the CMC has been observed previously.[33]

In contrast addition of methyl groups to the surfactant tails has a very pronounced effect. According to Traube's rule[50] each additional CH_2 group in the hydrophobic tail of an ionic surfactant decreases the CMC by a factor of two, which matches our observation (compare *e.g.* 9E2Q-3-Q2E9 with 11E2Q-3-Q2E11).

Insertion of a hydroxyl group in the linker modifies the trend described above as its presence reduces the CMC (compare 12Q-3(OH)-Q12 with 12Q-3-Q12 and 9E2Q-3(OH)-Q2E9 with 9E2Q-3-Q2E9). It has been suggested that the unexpectedly low CMC value of gemini surfactants with a hydroxyl group in the spacer is due to a more favorable packing in the micelles as a result of hydration of the hydroxyl group which favors a higher curvature.[51–54]

Nanorod synthesis

In order to compare the effect of several surfactants on nanoparticle growth, a set of standardized conditions is used. We have applied the method reported by Sau and Murphy,[39] where gold nanoparticle seeds are grown in the presence of cetyl trimethyl ammonium bromide (CTAB) into AuNRs with an AR of approximately 3.5 in a single growth step. A yield of rod-shaped particles greater than 95% is typically obtained. For comparison of surfactants with different CMC values, the surfactant concentration is kept constant at 50 times the CMC in clean water (see Experimental section for synthesis and analysis details).

We find that anisotropic growth is highly susceptible to small changes in the chemical structure of the surfactant. The data are summarized in Table 2, Fig. 1 and 2. In the following the key observations are highlighted.

Effect of tail length and structure

The absorption spectrum of particles prepared using surfactant 10Q-2-Q10 (Fig. 1A) shows two plasmon modes; a peak at 540 nm with a shoulder at 590 nm. Two plasmon bands suggest the presence of anisotropic particles as the high-energy band is attributed to the transversal direction (short axis) of the particles together with a contribution from isotropic particles, and the low-energy mode is attributed to the longitudinal direction (long axis).[55] The observation that the two bands are not well separated suggests that the particles have a very low AR. Indeed, the TEM images (Fig. 1B) confirm that the particles are short AuNRs with an AR of 1.6, produced in a 57% yield with the rest being mainly cubic structures (Table 2). Gemini 12Q-2-Q12 produces AuNRs in a better yield (72%), and with slightly higher AR, which is evident from the small red-shift of the longitudinal band compared to 10Q-2-Q10. In contrast, 14Q-2-Q14 only provides spherical particles, which is evident from the absorption spectrum showing a single band at 530 nm. Thus, increasing the tail length to 14 C-atoms gives no improvement in the yield of rods or aspect ratio. This observation may be explained by the fact that the solutions of 14Q-2-Q14 and 14Q-4-Q14 are highly viscous at the concentration used. It is well known that geminis with long tails and short spacers give high solution viscosity already at moderate surfactant concentration and this behavior has been attributed to the formation of cross-linked threadlike micelles.[29,30] Thus, for this series of geminis with a 2-carbon spacer there seems to be an optimum in tail length of 12 carbon atoms.

This finding may be compared with the results from a study where Murphy and co-workers[24] investigated a homologous series of single tail cationic surfactants, C_nTAB (n = 10, 12, 14, 16, and 18), with respect to the growth of high-aspect ratio AuNRs synthesized using a three-step procedure. They found that $C_{16}TAB$ yielded AuNRs with higher aspect ratio than the shorter and the longer tail surfactants. Thus, it seems that for gemini surfactants, as well as for conventional monomeric

Table 2 Size data for the anisotropic population of particles synthesized with different gemini surfactants as structure directing agents. The data were determined from 1000–8000 counts per sample

Surfactant[a]	η_{AuNR}[b] [%]	Aspect ratio	Length [nm]	Width [nm]	Sample morphology[c]
10Q-2-Q10	57	1.6 ± 0.3	26 ± 5	16 ± 3	R, C ≫ S and O
12Q-2-Q12	72	1.7 ± 0.3	29 ± 4	17 ± 2	R, C ≫ S and O
12Q-3-Q12	72	2.5 ± 0.7	35 ± 6	14 ± 3	R, C ≫ S and O
12Q-3(OH)-Q12	55	1.7 ± 0.3	17 ± 3	10 ± 1	R, C, S and O
12Q-4-Q12	72	2.3 ± 0.5	35 ± 6	16 ± 3	R, C ≫ S and O
12Q-6-Q12	79	1.9 ± 0.4	27 ± 6	14 ± 3	R > C ≫ S
14Q-2-Q14	4	1.3 ± 0.1	16 ± 2	12 ± 2	S
14Q-4-Q14	56	1.5 ± 0.3	23 ± 4	15 ± 3	O, R and C
9E2Q-3-Q2E9	70	1.7 ± 0.3	16 ± 2	9.4 ± 1	R, C and S
9E2Q-3(OH)-Q2E9	67	1.8 ± 0.3	17 ± 3	9.6 ± 1	R, C, S and O
9E2Q-6-Q2E9	79	2.7 ± 1.0	30 ± 9	12 ± 3	R ≫ S and C
11E2Q-3-Q2E11	18	1.4 ± 0.1	15 ± 2	11 ± 1	C and S ≫ R
11E2Q	86	1.9 ± 0.4	31 ± 6	16 ± 3	R ≫ C
CTAB	84	2.7 ± 0.9	34 ± 7	14 ± 4	R ≫ C

[a] All surfactant concentrations are 50× their respective CMC value. [b] Yield of rod-shaped objects defined as $\eta_{AuNR} = N_{AR>1.25}/(N_{AR>1.25} + N_{AR\leq1.25})$.
[c] General sample morphology: R = rods, C = cubes, S = spheres, and O = other shapes. Placed in order of dominance.
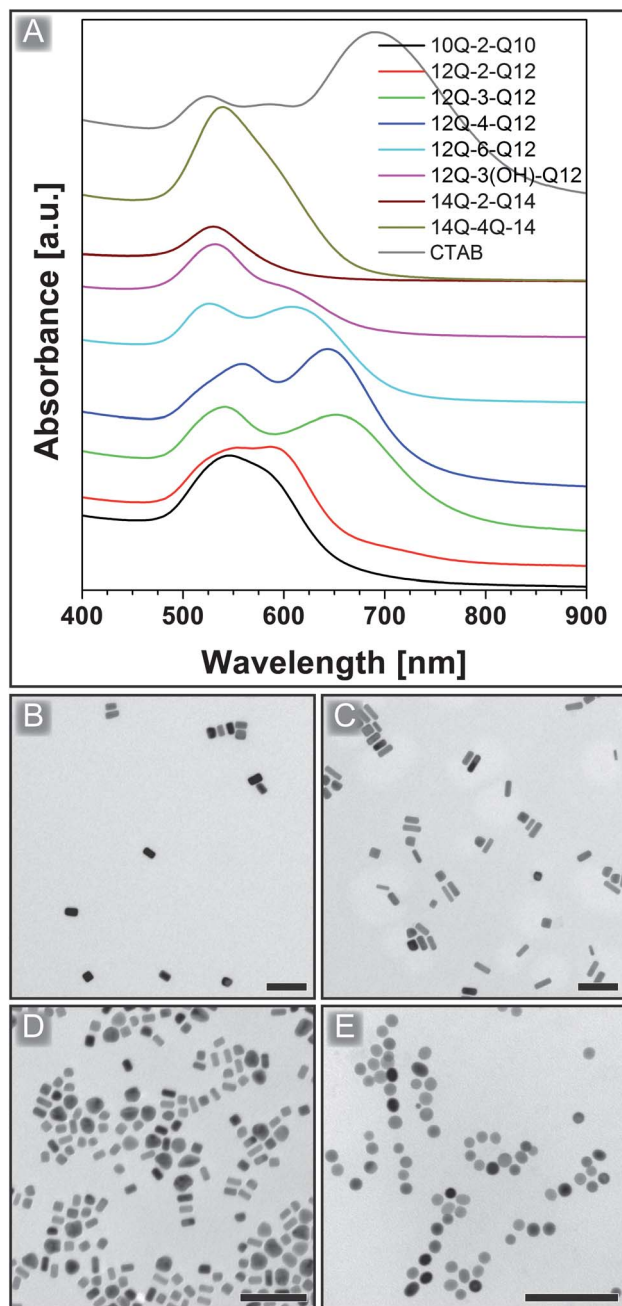
Fig. 1 Spectra and TEM images of nanoparticles prepared using gemini surfactants. (A) Absorption spectra. The spectra have been shifted vertically for clarity. TEM images of nanoparticles resulting from synthesis using (B) 10Q-2-Q10, (C) 12Q-3-Q12, (D) 12Q-3(OH)-Q12, and (E) 14Q-2-Q14. Scale bars are 100 nm.

Fig. 2 UV–vis and TEM images of nanoparticles stabilized with gemini surfactants having esterquat tails. (A) Absorption spectra. The spectra have been vertically shifted for clarity. (B–E) TEM images of nanoparticles resulting from synthesis using (B) 9E2Q-3-Q2E9, (C) 9E2Q-6-Q2E9, (D) 11E2Q-3-Q2E11, and (E) 11E2Q monomeric surfactant. Scale bars are 100 nm.

surfactants, there is an optimum in tail length. The presence of ester bonds in the surfactant tails is expected to increase the amount of packing disorder. However, no conclusive trend is observed in this study with respect to the yield and AR of AuNRs grown from ester-containing geminis; from the four ester-containing geminis one, 9E2Q-6-Q2E9, gave a high yield of AuNRs with a high AR; two, 9E2Q-3-Q2E9 and 9E2Q-3(OH)-Q2E9, gave moderate yields and moderate AR; and one, 11E2Q-3-Q2E11, gave poor yield and low AR. The surfactant structure
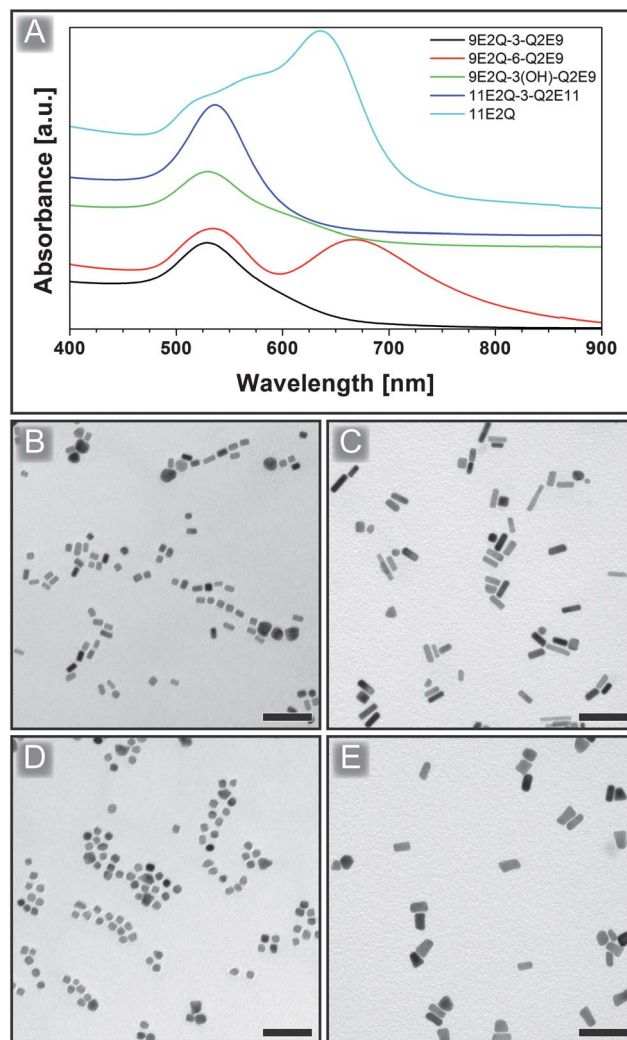
was varied with respect to the tail length (9E2Q-3-Q2E9 and 11E2Q-3-Q2E11), spacer length (9E2Q-3-Q2E9 and 9E2Q-6-Q2E9) and spacer group (9E2Q-3-Q2E9 and 9E2Q-3(OH)-Q2E9) – refer to Table 1 and Fig. 2. 9E2Q-3-Q2E9 forms rod-like particles with an AR of 1.7 in 70% yield, whereas the longer 11E2Q-3-Q2E11 results in mostly cubic and spherical particles, and only 18% yield of rods with a low AR of 1.4. The result here is similar to the alkyl gemini surfactants under study and regular monomeric surfactant without an ester bond in the tails;[24] too long tails prevent anisotropic nanoparticle growth. In comparison, the 11E2Q single-tail monomeric surfactant results in much higher yield (86%) of anisotropic particles, albeit a large component is oddly trapezoid-shaped gold nanoparticles (Fig. 2E). The high yield is reflected in the absorption spectrum (Fig. 2A), where the longitudinal absorbance is relatively large.
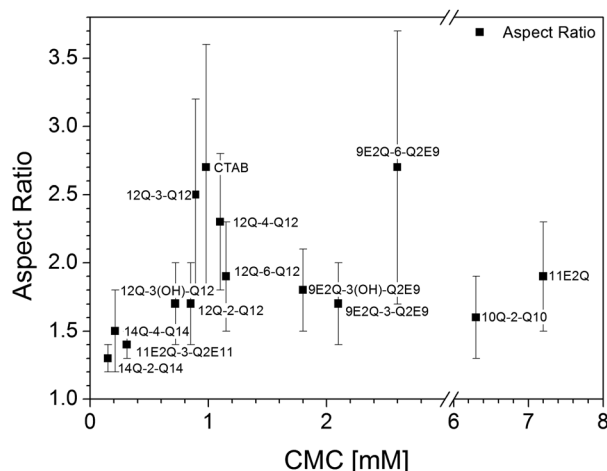
Fig. 3 Aspect ratio of the gold nanoparticles plotted against the CMC value of the respective surfactants.

Effect of spacer length and structure

Next, we turn our attention to the effect of the spacer length on the anisotropic growth. For the series 12Q-n-Q12 with $n = 2, 3, 4$ and 6 the influence of the spacer length on the aspect ratio (AR) was: $n = 2$: AR 1.7, $n = 3$: AR 2.5, $n = 4$: AR 2.3, and $n = 6$: AR 1.9. Thus, with respect to the aspect ratio, an optimum spacer length of 3 or 4 is observed.

Comparing 9E2Q-3-Q2E9 and 9E2Q-6-Q2E9 to study the effect of the spacer length of gemini surfactants with esterquat tails, it is observed that 9E2Q-6-Q2E9 forms high aspect ratio nanoparticles (AR 2.7, yield 79%) which is, in fact, the highest AR and the highest yield for any gemini surfactant used in this study (Fig. 2C). The larger AR is reflected in the absorption spectrum (Fig. 2A) in which the longitudinal component is located at 675 nm.

In order to change the polarity of the spacer unit a hydroxyl group was introduced on the central carbon of a 3-carbon chain. Two pairs, one with and one without a hydroxyl group, can be compared: 12Q-3-Q12 and 12Q-3(OH)-Q12, as well as 9E2Q-3-Q2E9 and 9E2Q-3(OH)-Q2E9. As is evident from Table 2, the
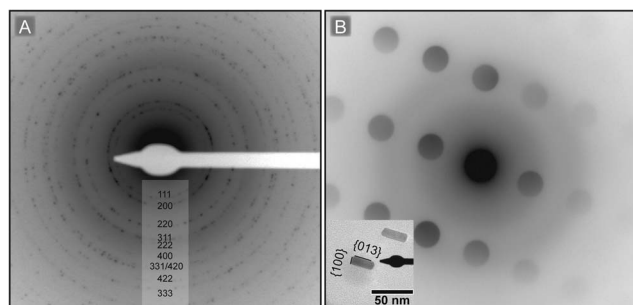

Fig. 4 (A) Selected area electron diffraction of AuNRs synthesized using 9E2Q-6-Q2E9 confirming a face-centered cubic lattice. (B) Typical {310} spot pattern of a single AuNR (inset) showing {100} and {310} faces. The diffraction patterns are compared with tables in ref. 58.

yield and the AR both decreased as a result of insertion of the hydroxyl group in the first pair. For the second pair the yield is slightly decreased whereas the AR remains unchanged when inserting an extra hydroxyl group. Thus, no clear effect of the hydroxyl group is observed in the aspect ratio, as was the case on the CMC, as discussed above.

Nanorod crystal structure

The crystallographic structure of AuNRs prepared from 9E2Q-6-Q2E9 was determined using SAED. The Au atoms are arranged in a face-centered cubic lattice, while spot patterns from single AuNRs show that they are single crystalline particles primarily dominated by {100} and {013} facets (Fig. 4).

Discussion

The relationship between the surfactant structure and the aspect ratio of the resulting nanorods can be summarized as follows: In order to maximize the AR (i) an optimum in tail alkyl chain length is observed for gemini surfactants as well as for regular monomeric surfactants, (ii) there is an effect on varying the length of the spacer unit, (iii) the presence of ester bonds in the hydrophobic tails yields inconsistent results, and so does (iv) the presence of a hydroxyl group in the spacer.

One interesting connection emerges from this relative broad collection of cationic surfactants, which is a correlation between the CMC of the surfactants and the AR (Fig. 3) and this correlation holds both for the gemini surfactants and for monomeric surfactants with the same polar head group. With the exception of 9E2Q-6-Q2E9, the AR exhibits a maximum for surfactants with a CMC of around 1 mM. Interestingly, the trend is the same for the CTAB homologues (tail length 10 to 18 carbon atoms) studied by Murphy and co-workers;[24] the CMC of the surfactant yielding the highest AR, $C_{16}TAB$ is 0.98 mM (ref. 38) as compared to the shorter $C_{14}TAB$ (CMC = 3.6 mM (ref. 38)) and longer $C_{18}TAB$ (CMC = 0.34 mM (ref. 38)) surfactants. The trend also holds for the gemini surfactants used by Liz-Marzan and co-workers[22,56] for synthesis of gold nano-rods, the PEG spaced gemini surfactant in that study was measured to have a CMC of 1.02 mM.

It needs to be stressed that CMCs are measured in distilled water. The conditions during AuNR growth are naturally different and consequently the CMC is shifted to lower values.

One may argue that the structure directing effect exerted by the surfactant must be related to self-assembly at the gold crystal surface, rather than its solution assembly behavior (which is described by the CMC). The gold surface exposed to quaternary ammonium surfactants with bromide as counterion can be regarded as a negatively charged surface.

A cationic surfactant used in high concentration (which is the case here) self-assembles on the surface either as closely packed micelles or as a double layer, the exact structure being dependent on the geometry of the surfactant.[57]

The thermodynamic driving force for self-assembly on the surface, namely the free energy gained in this process, should approximately scale with the driving force for self-assembly in

This journal is © The Royal Society of Chemistry 2014

J. Mater. Chem. C, 2014, **2**, 994–1003 | 999

the bulk, *i.e.* micelle formation. The results from this study indicate that there is an optimum driving force that maximizes the aspect ratio of AuNRs. If the free energy gain is too small (larger CMC) there is insufficient alignment of surfactant molecules, which is a prerequisite for directed growth. Too strong driving forces (small CMC) on the other hand might lead to excessive surface coverage preventing or at least considerably slowing down growth.

It is generally believed that the {100} facets, which constitute the sides of the growing gold rods, should be covered by a double layer of surfactants (or by closely packed micelles) whereas the ends, which are {111} facets, should not be covered by surfactants but instead be available for Au ions from the surrounding solution. If the tendency for the surfactant to self-assemble is very strong, it may also cover the {111} facet, thus slowing down or even preventing the anisotropic growth process.

Origin of {310} faceting

One experimental observation that we now seek to rationalize is the emergence of {310} surfaces at the cost of {100} and {110} surfaces when going from single head group to double head group (gemini) surfactants.

One can expect that the interaction of a strongly ionic surfactant such as CTAB with a metallic surface leads to considerable charge transfer. Such effects are of particular importance for understanding the stabilization of different surface orientations as discussed below and shown in Fig. 5C. Therefore opted to the present case we sacrifice dynamical (temperature) effects in favor of a more accurate description of the electronic structure. Here we have carried out an extensive investigation of alkyltrimethylammonium bromide molecules on several relevant Au surfaces using electronic structure calculations within density functional theory.

For computational convenience we have focused on butyltrimethylammonium bromide (BTAB) as a prototype for the surfactants used in the experimental part of this study. To select configurations we studied adsorption as a function of the tail length and found that absolute values for the adsorption energies for BTAB differ by less than 0.2 eV from CTAB with significantly smaller variations in the relative energy differences between.[59]

A low energy configuration representative of the adsorption of BTAB on {310} surfaces of Au is shown in Fig. 5b. It reveals two important features:

(i) Br atoms prefer adsorption sites above surface steps, an observation that appears to be general for Au surfaces as it occurs also on for example {111} or {110} surfaces. The migration barriers for Br atoms on {310} as well as on other {100} are calculated to be about 0.1 eV.

(ii) The butyltrimethylammonium cation hovers over the narrow {100} terraces. Translations or rotations of the cation with respect to the terrace surface normal only lead to small energy changes indicating smaller energy barriers than in the case of Br.

A key difference between AuNR growth using monomeric and gemini surfactants is the emergence of {310} side facets in the latter case at the cost of {110} and {250} facets.[31] To this end it is instructive to consider the geometries of clean surfaces of interest in the present study, an overview of which is provided in Fig. 6 illustrating the relationship between {100}, {110}, and {310} surfaces. In particular, note that the {310} surface can be considered as a {100} surface with a very high step density (steps oriented along {001}). Due to the preferential adsorption of Br at surface steps and an associated large adsorption energy, one can anticipate that BTAB (or CTAB) adsorption stabilizes surfaces with structural steps relative to flat surfaces. While this is an important indication it is not yet sufficient to explain the very pronounced preference for {310} observed for gemini surfactants.

A direct study of gemini surfactants using only electronic structure calculations at zero Kelvin is of limited relevance since at finite temperatures the linker will experience a substantial contraction due to entropic effects; hence the zero Kelvin adsorption geometry will not be representative. (Note that in the case of single head surfactants entropic effects are substantial for the tail but of much less significance for the head group.) Based on the results for BTAB adsorption and the comments regarding the presence of surface steps we can nonetheless formulate a growth mechanism that provides a rationale for the experimental observations.

In gemini surfactants two trimethylammonium type head groups are connected to each other *via* a linker (see Table 1). Furthermore, each of the two head groups is associated with one Br anion. One can thus imagine an adsorption geometry of the type schematically shown in Fig. 7A. Since the migration barriers for Br are larger than for the alkylammonium ion it is intuitive to approximate gemini adsorbates as stick-like with respect to the surface plane, where the end points of the stick correspond to the position of the Br atoms. Due to the strong preference of Br for step sites, gemini molecules should align
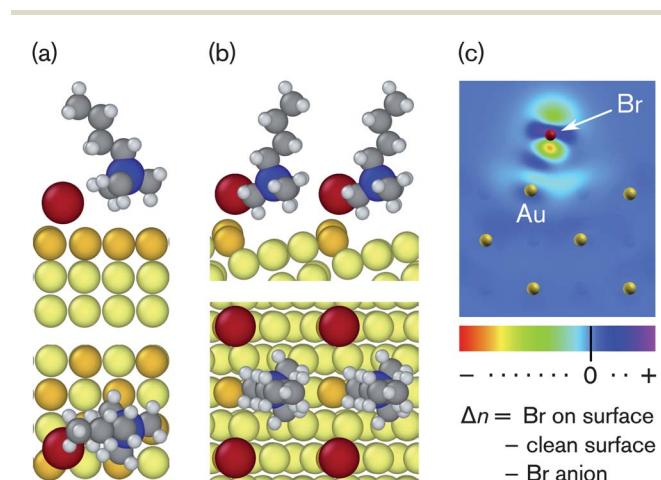

Fig. 5 Adsorption geometries of BTAB molecules on (A) {100} and (B) {310} surfaces at coverages of 1/4 and 1/2 in units of surface unit cells. (C) Planar cross-section of charge density difference between the {100} surface with Br adatom, clean surface and free Br anion. The figure illustrates the charge transfer between the anion and the surface.
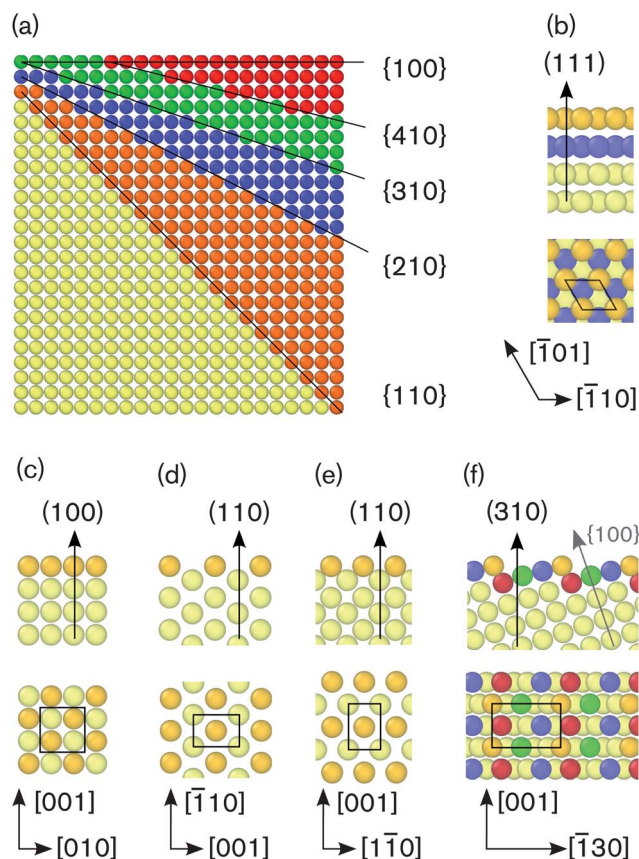
1000 | *J. Mater. Chem. C*, 2014, **2**, 994–1003

This journal is © The Royal Society of Chemistry 2014

Fig. 6 (A) Face-centered cubic lattice projected onto the {100} plane. The lines and colored regions indicate cuts generating different surface terminations between {100} and {110}. (B–F) Side (top row) and top (bottom row) views of (b) {100}, (c) {111}, (d and e) {110}, and (f) {310} surfaces. Coloring is used to help in the identification of different atomic layers.
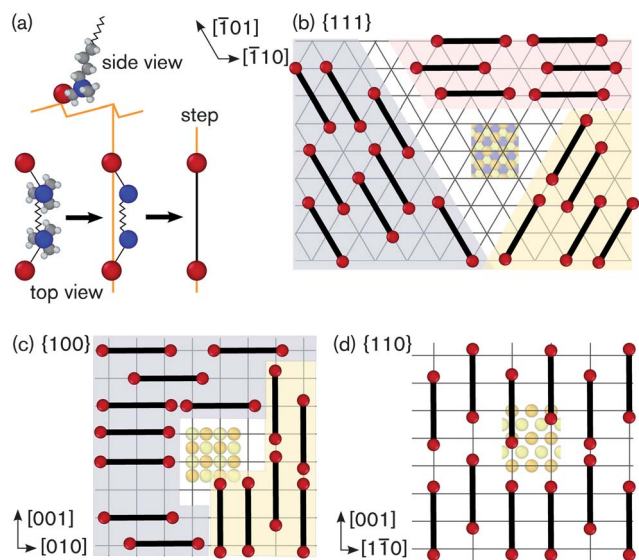

Fig. 7 (A) Simplified representation of gemini surfactants. (B–D) Suggested adsorption patterns of gemini surfactants on different surfaces. The solid lines indicate common directions for surface steps, the dumbbells represent individual gemini molecules, and the shaded regions indicate domains with parallel alignment of gemini surfactants.

with existing surface steps and even more so enhance their formation. Typical step directions are indicated by solid lines in Fig. 7B–D.

In a solution above the CMC, the chemical potential of BTAB (or CTAB) will be high and thus also the surface coverage. As a result of the steric repulsion between different surfactant molecules there is then a strong driving force for pattern formation by the gemini surfactants. Due to the correlation of gemini orientation with step orientation one can expect different types of patterns to form on different surfaces, as illustrated in Fig. 7B–D. It is apparent that this correlation triggers the formation of a pattern of parallel surface steps on {110} surfaces (see Fig. 7D, whereas on {111} and {100} surfaces domains with triangular and quadratic symmetry should emerge (Fig. 7B and C). Gold nanorods grown using CTAB (single head surfactants) exhibit {110} and {100} side facets. It has recently been shown that there are also higher index facets specifically {250} surfaces[31] this fact does not qualitatively alter our discussion.

As illustrated in Fig. 7, gemini surfactants will trigger the formation and parallel alignment of steps on these side facets. In the case of {111} and {100} surfaces several step directions are competing with each other, which should lead to frustration. In the case of {110} there is, however, only one possible alignment for {100} steps, which eventually leads to the emergence of miscut surface orientations such as {310}.

Based on these arguments one might still wonder why no other types of miscut surface orientations such as {410} or {510} are observed, which, as shown in Fig. 6A, would correspond to wider {100} terraces. A closer inspection of the energy landscape for Br on {310} surfaces shows that adsorption sites, which are not in the immediate vicinity of surface steps, are unstable. For these surfaces there are thus only adsorption sites at surface steps. As the width of the {100} terraces increases, as in the case of {410} and {510} surfaces, metastable Br adsorption sites become available in the center of the terraces. As soon as such a site is being occupied it can serve as a nucleation site and stabilizer for another surface step, the subsequent growth of which once again reduces the width of {100} terraces. Another factor is the size of the trimethylammonium head group, which, as can be seen in Fig. 6B, is comparable to the width of the terraces. One might therefore speculate that larger step widths could be stabilized by exploiting steric effects, *i.e.* by using surfactants with larger head groups. Other effects might, however, also lead to unstable growth under such conditions.

Conclusions

A library of gemini surfactants has been employed in the synthesis of anisotropic gold nanoparticles. Based on the observations of AR and AuNR yield, it can be concluded that there exist optimal structural parameters for the surfactants. The optimal tail length is found to be around 12 carbon atoms. Effects of the spacer length and type are less conclusive. Interestingly, by comparing all surfactants in this study together with similar surfactants reported by others[24,22] it is found that surfactants furnishing rods in high yield and AR all had a CMC

close to 1 mM. The only exception to this trend among the gemini surfactants considered in this study is E2Q-6-Q2E9 yielding an aspect ratio of 2.7 and a nanorod yield of 79%.

We attribute this observation to the fact that there exists an optimum CMC for surfactant directed anisotropic gold nanorod growth.

Gold nanorods grown using gemini surfactants exhibit {310} side facets rather than more commonly {110}, {100}, or {250} surfaces. We rationalize this observation on the basis of electronic structure calculations, which show a pronounced preference for Br adsorption at step edges. In combination with the geometry of gemini surfactants this suggests a picture, in which gemini surfactants stabilize surface steps leading to their respective alignment and eventually the emergence of the miscut {310} surfaces.

We note that monomeric surfactants such as C_{16}TAB furnish AuNRs in higher yield and aspect ratio when compared to the results obtained with gemini surfactants. Based on these observations it seems reasonable to conclude that the detailed chemical binding energy and geometry of the surfactant head group at the gold surface is more important than the "templating effect" induced by elongated micelles. Future design of new surfactants for anisotropic noble metal crystal growth should therefore focus on engineering the structure of the head group.

Acknowledgements

References

1 F. Westerlund and T. Bjørnholm, *Curr. Opin. Colloid Interface Sci.*, 2009, **14**, 126–134.

2 C. J. Murphy, L. B. Thompson, D. J. Chernak, J. A. Yang, S. T. Sivapalan, S. P. Boulos, J. Huang, A. M. Alkilany and P. N. Sisco, *Curr. Opin. Colloid Interface Sci.*, 2011, **16**, 128–134.

3 S. M. Marinakos, S. Chen and A. Chilkoti, *Anal. Chem.*, 2007, **79**, 5278–5283.

4 C. J. Murphy, A. M. Gole, S. E. Hunyadi, J. W. Stone, P. N. Sisco, A. Alkilany, B. E. Kinard and P. Hankins, *Chem. Commun.*, 2008, 544–557.

5 A. C. Bonoiu, S. D. Mahajan, H. Ding, I. Roy, K.-T. Yong, R. Kumar, R. Hu, E. J. Bergey, S. A. Schwartz and P. N. Prasad, *Proc. Natl. Acad. Sci. U. S. A.*, 2009, **106**, 5546–5550.

6 D. Pissuwan, T. Niidome and M. B. Cortie, *J. Controlled Release*, 2011, **149**, 65–71.

7 T. Jain, F. Westerlund, E. Johnson, K. Moth-Poulsen and T. Bjørnholm, *ACS Nano*, 2009, **3**, 828–834.

8 T. Jain, R. Roodbeen, N. E. A. Reeler, T. Vosch, K. J. Jensen, T. Bjørnholm and K. Nørgaard, *J. Colloid Interface Sci.*, 2012, **376**, 83–90.

9 Q. Tang, Y. Tong, T. Jain, T. Hassenkam, Q. Wan, K. Moth-Poulsen and T. Bjørnholm, *Nanotechnology*, 2009, **20**, 245205.

10 T. Jain, Q. Tang, T. Bjørnholm and K. Nørgaard, *Acc. Chem. Res.*, 2013, DOI: 10.1021/ar3002848.

11 T. A. Gschneidtner, Y. A. Diaz Fernandez and K. Moth-Poulsen, *J. Mater. Chem. C*, 2013, **1**, 7127–7133.

12 T. Jain, S. Lara-Avila, Y.-V. Kervennic, K. Moth-Poulsen, K. Nørgaard, S. Kubatkin and T. Bjørnholm, *ACS Nano*, 2012, **6**, 3861–3867.

13 A. Rey, G. Billardon, E. Lörtscher, K. Moth-Poulsen, N. Stuhr-Hansen, H. Wolf, T. Bjørnholm, A. Stemmer and H. Riel, *Nanoscale*, 2013, **5**, 8680–8688.

14 N. R. Jana, L. Gearheart and C. J. Murphy, *J. Phys. Chem. B*, 2001, **105**, 4065–4067.

15 B. Nikoobakht and M. A. El-Sayed, *Chem. Mater.*, 2003, **15**, 1957–1962.

16 R. Becker, B. Liedberg and P.-O. Käll, *J. Colloid Interface Sci.*, 2010, **343**, 25–30.

17 S. Koeppl, C. Solenthaler, W. Caseri and R. Spolenak, *J. Nanomater.*, 2011, **2011**, 1–13.

18 B. D. Busbee, S. O. Obare and C. J. Murphy, *Adv. Mater.*, 2003, **15**, 414–416.

19 N. Garg, C. Scholl, A. Mohanty and R. Jin, *Langmuir*, 2010, **26**, 10271–10276.

20 D. K. Smith, N. R. Miller and B. A. Korgel, *Langmuir*, 2009, **25**, 9518–9524.

21 M. Liu and P. Guyot-Sionnest, *J. Phys. Chem. B*, 2005, **109**, 22192–22200.

22 A. Guerrero-Martínez, J. Pérez-Juste, E. Carbó-Argibay, G. Tardajos and L. M. Liz-Marzán, *Angew. Chem., Int. Ed.*, 2009, **48**, 9484–9488.

23 L. Li, Z. Wang, T. Huang, J. Xie and L. Qi, *Langmuir*, 2010, **26**, 12330–12335.

24 J. Gao, C. M. Bender and C. J. Murphy, *Langmuir*, 2003, **19**, 9065–9070.

25 G. Grochola, I. K. Snook and S. P. Russo, *J. Chem. Phys.*, 2007, **127**, 194707.

26 J. Feng, R. B. Pandey, R. J. Berry, B. L. Farmer, R. R. Naik and H. Heinz, *Soft Matter*, 2011, 7, 2113.

27 a. S. Barnard and L. a. Curtiss, *J. Mater. Chem.*, 2007, **17**, 3315.

28 C. J. Murphy, T. K. Sau, A. M. Gole, C. J. Orendorff, J. Gao, L. Gou, S. E. Hunyadi and T. Li, *J. Phys. Chem. B*, 2005, **109**, 13857–13870.

29 D. Danino, Y. Talmon and R. Zana, *Langmuir*, 1995, **11**, 1448–1456.

30 A. Bernheim-Groswasser, R. Zana and Y. Talmon, *J. Phys. Chem. B*, 2000, **104**, 4005–4009.

31 E. Carbó-Argibay, B. Rodríguez-González, S. Gómez-Graña, A. Guerrero-Martínez, I. Pastoriza-Santos, J. Pérez-Juste and L. M. Liz-Marzán, *Angew. Chem.*, 2010, **122**, 9587–9590.

32 S. Gómez-Graña, J. Pérez-Juste, R. a. Alvarez-Puebla, A. Guerrero-Martínez and L. M. Liz-Marzán, *Adv. Opt. Mater.*, 2013, **1**, 477–481.

33 R. Zana, M. Benrraou and R. Rueff, *Langmuir*, 1991, 7, 1072–1075.

1002 | *J. Mater. Chem. C*, 2014, **2**, 994–1003

This journal is © The Royal Society of Chemistry 2014

34 A. R. Tehrani-Bagha, H. Oskarsson, C. G. van Ginkel and K. Holmberg, *J. Colloid Interface Sci.*, 2007, **312**, 444–452.

35 A. R. Tehrani-Bagha and K. Holmberg, *Langmuir*, 2010, **26**, 9276–9282.

36 M. J. Rosen and L. D. Song, *J. Colloid Interface Sci.*, 1996, **179**, 261–268.

37 A. Tehrani-Bagha, J. Kärnbratt, J.-E. Löfroth and K. Holmberg, *J. Colloid Interface Sci.*, 2012, **376**, 112–118.

38 M. J. Rosen, *Surfactants and Interfacial Phenomena*, Wiley-Blackwell, 3rd edn, 2004.

39 T. K. Sau and C. J. Murphy, *Langmuir*, 2004, **20**, 6414–6420.

40 A. Gole and C. J. Murphy, *Chem. Mater.*, 2004, **16**, 3633–3640.

41 C. Igathinathane, L. Pordesimo, E. Columbus, W. Batchelor and S. Methuku, *Comput. Electron Agr.*, 2008, **63**, 168–182.

42 P. Blöchl, *Phys. Rev. B: Condens. Matter Mater. Phys.*, 1994, **50**, 17953.

43 G. Kresse and D. Joubert, *Phys. Rev. B*, 1999, **59**, 11–19.

44 G. Kresse and J. Hafner, *Phys. Rev. B*, 1993, **47**, 558–561.

45 G. Kresse and J. Furthmüller, *Phys. Rev. B: Condens. Matter Mater. Phys.*, 1996, **54**, 11169–11186.

46 G. Kresse and J. Furthmüller, *Phys. Rev. B*, 1996, **6**, 15–50.

47 J. Perdew, K. Burke and M. Ernzerhof, *Phys. Rev. Lett.*, 1996, **77**, 3865–3868.

48 F. M. Menger and C. Littau, *J. Am. Chem. Soc.*, 1991, **113**, 1451–1452.

49 M. J. Rosen and D. Tracy, *J. Surfactants Deterg.*, 1998, **1**, 547–554.

50 K. Holmberg, B. Jönsson, B. Kronberg and B. Lindman, *Surfactants and polymers in aqueous solution*, John Wiley & Sons Ltd., 2nd edn, 2003.

51 M. Rosen, *J. Am. Oil Chem. Soc.*, 1996, **73**, 885–890.

52 T. S. Kim, T. Kida, Y. Nakatsuji, T. Hirao and I. Ikeda, *J. Am. Oil Chem. Soc.*, 1996, **73**, 907–911.

53 X. Pei, Y. You, J. Zhao, Y. Deng, E. Li and Z. Li, *J. Colloid Interface Sci.*, 2010, **351**, 457–465.

54 S. Wettig, P. Nowak and R. Verral, *Langmuir*, 2002, **18**, 5354–5359.

55 J. Pérez-Juste, I. Pastoriza-Santos, L. M. Liz-Marzán and P. Mulvaney, *Coord. Chem. Rev.*, 2005, **249**, 1870–1901.

56 S. D. Wettig, X. Li and R. E. Verrall, *Langmuir*, 2003, **19**, 3666–3670.

57 R. Atkin, V. S. J. Craig, E. J. Wanless and S. Biggs, *J. Colloid Interface Sci.*, 2003, **266**, 236–244.

58 J. W. Edington, Practical Electron Microscopy in *Materials Science - 2. Electron Diffraction in the Electron Microscope*, The Macmillan Press LTD., 1975.

59 R. Crawford, masters thesis, Chalmers, 2013.

This journal is © The Royal Society of Chemistry 2014

J. Mater. Chem. C, 2014, **2**, 994–1003 | **1003**